YJMRE 3415 ARTICLE IN PRESS No. of Pages 16; 4C: 13, Model 5+
29 November 2005 Disk Used Leo (CE) / Vijaykumar (TE)

Available online at www.sciencedirect.com
SCIENCE DIRECT®
ELSEVIER
Journal of Magnetic Resonance xxx (2005) xxx–xxx
JMR Journal of Magnetic Resonance
www.elsevier.com/locate/jmr

Two-dimensional hyperfine sublevel correlation spectroscopy: Powder features for $S = 1/2$, $I = 1$

Alexander G. Maryasov [a,b,*], Michael K. Bowman [b]

[a] Institute of Chemical Kinetics and Combustion, Siberian Branch of Russian Academy of Sciences, Novosibirsk 630090, Russian Federation
[b] Structural Biology and Microimaging, Battelle Northwest, Richland, WA 99354, USA

Received 26 August 2005; revised 20 November 2005

Abstract

The lineshapes of two-dimensional magnetic resonance spectra of disordered or partially ordered solids are dominated by ridges of singularities in the frequency plane. The positions of these ridges are described by a branch of mathematics known as catastrophe theory concerning the mapping of one 2D surface onto another. We systematically consider the characteristics of HYSCORE spectra for paramagnetic centers having electron spin $S = 1/2$ and nuclear spin $I = 1$ in terms of singularities using an exact solution of the nuclear spin Hamiltonian. The lineshape characteristics are considered for several general cases: zero nuclear quadrupole coupling; isotropic hyperfine but arbitrary nuclear quadrupole couplings; coincident principal axes for the nuclear hyperfine and quadrupole tensors; and the general case of arbitrary nuclear quadrupole and hyperfine tensors. The patterns of singularities in the HYSCORE spectra are described for each case.

Keywords: ESE EM; HYSCORE; 2D spectroscopy; Catastrophe theory; Nitrogen nucleus; Hyperfine interaction; Singularity patterns; Mapping; Quadrupolar interaction; Fold; Cusp

1. Introduction

Techniques to allow observation of multidimensional spectra are widely applied in magnetic resonance spectroscopy for better resolution and easier interpretation of experimental data [1,2]. Two-dimensional (2D) displays of spectra are used extensively because they are readily visualized. In both electron paramagnetic resonance and nuclear magnetic resonance (EPR and NMR) spectroscopies, 2D spectra are obtained as slices or projections of higher dimensional spectra or by applying some pulse sequence to the system in question where two time intervals, t_1 and t_2, in the pulse sequence are varied independently, see Fig. 1. The system response (typically spin echo or free induction signal) is stored as a 2D array of data. After 2D Fourier transformation, one obtains the 2D spectral density of the signal in the ω_1, ω_2 plane, where the frequency, ω_j, is the Fourier conjugate of t_j. In solid state measurements, such spectra often have complicated lineshapes because of anisotropic interactions that cause molecules with different orientations to have different spectral frequencies. If the molecules in the sample have complete or partial orientational disorder, (often referred to as 'powder' samples), the detailed lineshapes offer an opportunity to determine the complete, anisotropic magnetic resonance parameters of the molecule (see, e.g. [3,4]).

In 2D Fourier magnetic resonance experiments, the time-domain signal produced by molecules at any single, arbitrary orientation may be presented as

$$V(t_1, t_2) = \sum_{j,k=1}^{N} A_{j,k} \exp(\imath\Omega_j t_1 + \imath\Omega_k t_2), \qquad (1)$$

where the frequencies Ω_j depend on the spin Hamiltonian eigenvalues and in simple cases are the transition frequencies of the system. The amplitudes, $A_{j,k}$, depend on the

* Corresponding author. Fax: +7 383 330 7350.
E-mail address: maryasov@ns.kinetics.nsc.ru (A.G. Maryasov).

1090-7807/$ - see front matter © 2005 Published by Elsevier Inc.
doi:10.1016/j.jmr.2005.11.013

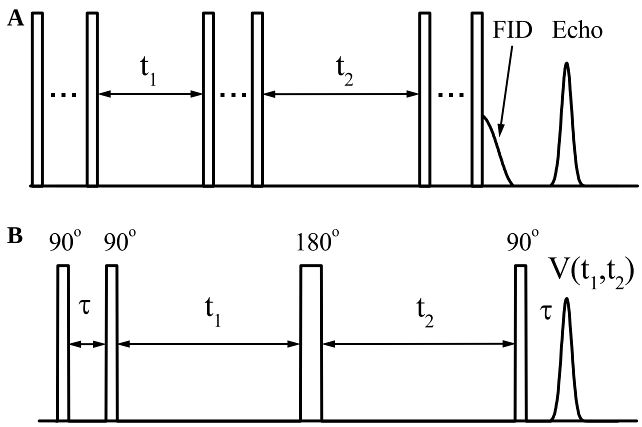

Fig. 1. Pulse sequences used in two-dimensional spectroscopy, (A) the general scheme, and (B) HYSCORE experiment implementation. In the latter case the stimulated echo signal amplitude is measured. It is generated by the first, second and the fourth pulses. The signal amplitude is measured as a function of two delays, t_1 and t_2, between the mixing (third) pulse and second and fourth pulses, respectively. The rotation angles are shown above the pulses.

characteristics of the microwave (mw) pulses in the case of EPR or radiofrequency (rf) pulses in the case of NMR, the particular pulse sequence, and on the parameters of the spin Hamiltonian. Both Ω_j and $A_{j,k}$ implicitly depend on the orientation of the molecule in the magnetic field of the spectrometer because the spin Hamiltonian generally is orientation dependent. In this paper, we use a type of 2D EPR spectroscopy known as HYSCORE [7] as a specific example, although the approach is applicable to other types of 2D EPR [8–10] or NMR methods. For simplicity, we do not consider relaxation in Eq. (1) and assume both frequencies to be non-zero. In general, the signal described by Eq. (1) consists of damped periodic oscillations in the time domain. We ignore the damping here because it is usually negligible compared to damping caused by interference from the distribution of frequencies in a 'powder' sample.

Fourier transformation of Eq. (1) gives

$$V_{\mathrm{F}}(\omega_1,\omega_2)=\sum_{j,k=1}^{N}A_{j,k}\delta(\omega_1-\Omega_j)\delta(\omega_2-\Omega_k), \tag{2}$$

where $\delta(x)$ is Dirac's delta-function. Instead of a smooth function of two variables in the time domain, the transformed signal is a set of discrete points in the frequency domain having infinite amplitude and zero spectral density in the rest of the frequency plane. For an orientationally disordered or 'powder' sample, Eqs. (1) and (2) must be integrated over the orientations of the molecules in the sample with respect to the laboratory frame. Such integration leads to a set of regions or spectral 'lines' having non-zero spectral density, which may partly overlap each other. The boundaries between regions with zero and non-zero spectral density often form rather prominent ridges. Such 2D patterns of ridges allow precise determination of the spin Hamiltonian parameters from which valid inferences of the molecular or electronic structure can be made and is the motivation for the use of 'contour lineshapes' developed by Dikanov [5]. In favorable cases, spin Hamiltonian parameters are determined completely by the positions of the ridges without the need to consider the intensity factors in Eqs. (1) and (2). This paper systematically examines the shapes of these ridges and the question of whether prominent ridges lie only on the boundaries between regions with and without spectral density.

From the point of view of mathematics, each term in Eq. (2) represents a smooth mapping of the hemisphere of possible orientations onto the frequency plane

$$\begin{cases}\omega_1=\Omega_j(\theta,\phi)\\ \omega_2=\Omega_k(\theta,\phi)\end{cases}. \tag{3}$$

Here θ and ϕ are the polar and azimuthal angles relating the external magnetic field to the molecular frame. Because inversion of the magnetic field does not change the eigenvalues of the spin-Hamiltonian, only a hemisphere of possible orientations need be considered. We will make extensive use of the unit hemisphere defined by θ and ϕ in discussing the orientation dependence of the spectral frequencies in the 2D spectra. This smooth mapping generates singularities where many orientations of a paramagnetic center (PC) result in the same set of frequencies so that significant areas of the hemisphere map to a single, intense point in the frequency plane.

These singularities produce a 2D 'powder' spectrum with prominent features where the signal intensity approaches infinity in the ideal case. The branch of mathematics which concerns singularities in the smooth mappings of one metric space onto the other is called catastrophe theory [6]. We used catastrophe theory to predict and understand features in HYSCORE spectra for different classes of spin Hamiltonians but for this paper we try to explain those results with more familiar mathematics. Other approaches have been used with great success (see the excellent discussion of 2D NMR powder lineshapes in [S-R & S]).

In HYSCORE spectra, the singularities are modified by the intensity factor, $A_{j,k}$. The intensity factor is strictly bounded, generally, $0 \leqslant |A_{j,k}|^2 \leqslant 1$. These intensity factors may cause part of a singularity to have zero amplitude, but they can never produce a singularity independent of the mapping. Thus, the prominent features in a spectrum correspond to singularities whose locations can be determined without calculating the $A_{j,k}$ although not every singularity will have sufficient intensity to be observed.

This paper considers 2D spectroscopy in 'powder' samples in the context of catastrophe theory and focuses on the features of the spectrum that arise from singularities produced by the mapping because in many cases the locations of these singularities are sufficient to determine the desired spin Hamiltonian parameters. A form of 2D pulsed EPR spectroscopy, known as hyperfine sublevel correlation (HYSCORE) spectroscopy [7], of PCs having electron spin $S=1/2$ and nuclear spin $I=1$ is used as a specific spectroscopic example. HYSCORE uses the electron spin for the indirect detection of nuclear spin coherences generated in nuclei with an appreciable hyperfine coupling to the PC.

Our analysis is based on exact solutions of the complete nuclear spin Hamiltonians. Although the discussion is in the context of HYSCORE spectroscopy, it is directly relevant to other forms of pulsed EPR spectroscopy, for example, 2D TRIPLE [8,9], 2D ENDOR ESEEM correlation spectroscopy [8] or double nuclear coherence transfer (DONUT)-HYSCORE spectroscopy [10]. Catastrophe theory has been used in the theory of nonlinear resonances in molecular spectroscopy (see, e.g. [11]) and in ferromagnetic resonance spectra [12].

The origin of the nuclear quantum beats in pulsed EPR experiments such as HYSCORE will be outlined first, followed by a few important results from catastrophe theory relevant to this paper. Then the 2D 'powder' lineshapes in HYSCORE spectra will be considered for several general classes of spin Hamiltonians. Although numerical simulations of HYSCORE spectra have been made for specific sets of spin Hamiltonian parameters and analytical results obtained for the simpler cases, this is the first systematic investigation of the locations of the singularities and the methods to rapidly calculate their locations.

2. Electron spin echo envelope modulation and HYSCORE spectra

The effect of electron spin echo (ESE) envelope modulation (EM) [13,14] was discovered about four decades ago and is a periodic oscillation in the electron spin echo signal amplitude as the time interval between microwave pulses is varied. Electron spin flips produced by nonselective mw pulses change the local magnetic field produced by the hyperfine interaction (hfi) at a nearby nucleus. These instantaneous changes in local field generate interfering nuclear coherences or, in other words, quantum beats in the nuclear subsystem. These quantum beats give rise in ESE experiments to an amplitude modulation of the echo known as EM.

Let us consider the EM in detail using a vector model we originally defined for the case of $S = 1/2$, $I = 1/2$ and which we now extend to $S = 1/2$, $I = 1$. The system Hamiltonian (in units of angular frequency) consists of three terms

$$\hat{H} = \hat{H}_S + \hat{\vec{S}}\overleftrightarrow{A}\hat{\vec{I}} + \hat{H}_I, \tag{4}$$

where the first and the third terms depend on the electron and nuclear spin operators, respectively, and the second term describes the electron—nuclear hfi with $\overleftrightarrow{A}$ being the tensor of this interaction. In the case of (effective) electron spin, $S = 1/2$, H_S reduces to the electron Zeeman interaction. In many cases, the quantization axis for the electron spin coincides with the direction of the external magnetic field $\vec{k}_z$ (this direction is chosen as the z axis of the laboratory frame) with high accuracy so the first and the second terms in the Hamiltonian (4) may be written in the form

$$\hat{H}_S + \hat{\vec{S}}\overleftrightarrow{A}\hat{\vec{I}} \approx \omega_S \hat{S}_z + \hat{S}_z(\vec{A}\cdot\hat{\vec{I}}) \tag{5}$$

for the typical 'high field' limit in which $|\hat{H}_S| \gg |\hat{\vec{S}}\overleftrightarrow{A}\hat{\vec{I}}|, |\hat{H}_I|$. Here the vector $\vec{A}$ is proportional to the hyperfine field produced at the nucleus by the electron spin

$$\vec{A} = \vec{k}_z \overleftrightarrow{A}\,. \tag{6}$$

The approximation (5) allows factorization of the system eigenfunctions as a product of wavefunctions, $|\psi\rangle = |m_S\rangle|\psi_{I,m_S}\rangle$, where the second term in the product is the eigenfunction of the nuclear subhamiltonian, $\hat{H}_{I,m_S}$, corresponding to a manifold of states with m_S being the projection of the electron spin onto its quantization axis, in our case $m_S = \pm 1/2$. This operator may be written as

$$\hat{H}_{I,m_S} = m_S\vec{A}\cdot\hat{\vec{I}} + \hat{H}_I = \omega_I\hat{I}_z + m_S\vec{A}\cdot\hat{\vec{I}} + \hat{\vec{I}}\overleftrightarrow{Q}\hat{\vec{I}}. \tag{7}$$

Here ω_I is the nuclear Zeeman frequency and $\overleftrightarrow{Q}$ is the nuclear quadrupolar interaction tensor. Electron spin flips induced by mw pulses change the value of m_S in Eq. (7) and can project eigenstates of $\hat{H}_{I,1/2}$, for example, into a coherent superposition of eigenstates of $\hat{H}_{I,-1/2}$, giving rise to the quantum beats.

For spin $I = 1$, the Hamiltonian (7) was solved in a series of papers by Muha [15] in trigonometric form. The eigenvalues may be written as

$$\Omega_{m_S,j} = \left(\frac{4|p_{m_S}|}{3}\right)^{1/2}\cos\left[\frac{\lambda_{m_S} + 2\pi j}{3}\right] \tag{8}$$

for $j = 0, 1, 2$ and

$$\cos\lambda_{m_S} = \frac{q_{m_S}}{2}\left(\frac{3}{|p_{m_S}|}\right)^{3/2}, \tag{9}$$

where (see also our earlier paper [16])

$$p_{m_S} = -\left[D_{m_S}^2 + \kappa^2(3 + \eta^2)\right], \tag{10}$$

$$q_{m_S} = \vec{D}_{m_S}\overleftrightarrow{Q}\vec{D}_{m_S} - 2\kappa^3(1 - \eta^2). \tag{11}$$

Here $\vec{D}_{m_S}$ is the effective field (in units of an angular frequency) affecting the nuclear spin, given by the vector sum of the external magnetic field and the hyperfine field

$$\vec{D}_{m_S} = \omega_I\vec{k}_z + m_S\vec{A} \tag{12}$$

and D_{m_S} is its length. The nuclear quadrupole interaction tensor is often written as

$$\overleftrightarrow{Q} = \begin{bmatrix} -(1-\eta)\kappa & 0 & 0 \\ 0 & -(1+\eta)\kappa & 0 \\ 0 & 0 & 2\kappa \end{bmatrix} \tag{13}$$

in the frame of its principal axes, here κ is the quadrupolar coupling constant, and η is the asymmetry parameter.

The four pulse sequence producing the HYSCORE spectra is shown in Fig. 1B. The measured signal is the stimulated echo amplitude generated by the 1st, 2nd, and 4th pulses as a function of the two delays t_1 (between the 2nd and the 3rd inverting pulse) and t_2 (between the 3rd and the 4th pulses) as shown in the figure. In this case, the 2D spectral density given by Eq. (2) for a PC having a particular orientation may be written as

$$V_{\mathrm{F}}(\omega_1,\omega_2)=\sum_{n,j,r,s}\delta(\omega_1-\Omega_\alpha^{j,n})\delta(\omega_2-\Omega_\beta^{r,s})A_{njrs}(\theta,\phi)+\sum_{n,j,r,s}\delta(\omega_1-\Omega_\beta^{j,n})\delta(\omega_2-\Omega_\alpha^{r,s})B_{njrs}(\theta,\phi), \qquad (14)$$

where the transition frequencies of the nuclear subhamiltonians are [15,16]

$$\Omega_{m_S}^{j,k}=\Omega_{m_S,j}-\Omega_{m_S,k}=2|p_{m_S}|^{1/2}\mathrm{sgn}[k-j]\xi_{m_S,j+k} \qquad (15)$$

with

$$\xi_{m_S,n}=\sin\left[\frac{\lambda_{m_S}+\pi n}{3}\right] \qquad (16)$$

being a dimensionless factor, α and β are used here and below instead of $m_S=+1/2$ and $m_S=-1/2$, respectively, for better readability. The number n ($n=1,2,3$) in Eq. (16) indexes the three possible transitions in the spectrum of the nucleus [15,16]. The largest transition frequency occurs for $n=1$ and is often called the double quantum (dq) transition while the $n=2$ and 3 transitions are called single quantum (sq) transitions. The amplitudes A and B may be calculated in the framework of the standard description of HYSCORE [2,5] using the Mims matrices [17], M, whose elements are scalar products of nuclear eigenfunctions belonging to different electron spin manifolds, or using the spectral decomposition of subhamiltonians from Eq. (7) as developed in [16]. In the latter case, only the eigenvalues are needed for the calculations. In this paper, the explicit forms of the amplitudes are of no importance, only the fact that their magnitude is less than unity.

Each product of delta-functions in Eq. (14) maps the hemisphere of orientations onto the frequency plane. Each product correlates transition frequencies from two different electron spin manifolds, providing an opportunity to extract the parameters of the nuclear subhamiltonians. There are 72 terms in Eq. (14) for $I=1$ that map onto 72 distinct but often overlapping regions of the entire frequency plane. Each term maps the unit hemisphere into a single, continuous region whose outline is a singularity. Because of the symmetry of the HYSCORE spectra [2] usually only the $\omega_2\geqslant 0$ half-plane with 36 ridges is displayed.

Let us consider one term from Eq. (14), for example, the one with the coefficient A_{njrs}. The appropriate mapping will be:

$$\omega_1=\Omega_\alpha^{j,n}(\theta,\phi),\qquad \omega_2=\Omega_\beta^{r,s}(\theta,\phi). \qquad (17)$$

The singularities produced by this mapping provide the region with fine structure consisting of one or a few ridges where the spectral density goes to infinity. Any ridge may cross itself or another ridge from the same or a different region. In Section 4, we consider in detail the patterns that these ridges form for several general types of nuclear spin Hamiltonians.

3. Relevant results from catastrophe theory

Eq. (17) describes a smooth mapping (since ω_1 and ω_2 are functions of θ and ϕ) $R_2\Rightarrow R_2$, where R_i is an i-dimensional metric space. All possible singularities resulting from such a mapping in the general case were described in the paper by Whitney half-a-century ago [18]. The theory of singularities of smooth mappings of multidimensional spaces forms a part of catastrophe theory together with the theories of caustics of wave fronts and bifurcations of solutions of ordinary nonlinear differential equations [6], where similar objects appear.

For us, the most important result is the discovery by Whitney [18] that, in the general case, only two types of singularities exist. Whitney called these folds and cusps, see Fig. 2 for examples. An example of a fold is the projection of a sphere onto a plane. Each point on the plane near the fold singularity corresponds to zero or two points on the surface of the sphere. The case of a cusp is less simple; it may be described as the junction of two annihilating folds. Near a cusp, each point on most of the plane corresponds to only one point of the projected surface while inside a narrow angle each point on the plane corresponds to three points on the projected surface with fold singularities meeting at a cusp separating these regions of the plane. More complex singularities are special cases that may be reduced to a set of folds and cusps by arbitrarily small distortions of the projected surface bringing it into a condition known as a "general position." The singularity that forms the outline of a spectral region cannot contain a cusp because there must be at least one point of the surface on either side of a cusp while no point on the unit hemisphere can be projected outside the spectral region. This means that any cusps that exist must lie in the interior of the HYSCORE line.

The singularities in the mapping (17) obey a simple equation obtained from catastrophe theory or the calculus of coordinate transformations [4]. That is, the Jacobian, J, of the mapping vanishes on these lines

$$J=\frac{\partial\left(\Omega_\alpha^{j,n}(\theta,\phi),\Omega_\beta^{r,s}(\theta,\phi)\right)}{\partial(\theta,\phi)}=\frac{\partial\Omega_\alpha^{j,n}}{\partial\theta}\frac{\partial\Omega_\beta^{r,s}}{\partial\phi}-\frac{\partial\Omega_\alpha^{j,n}}{\partial\phi}\frac{\partial\Omega_\beta^{r,s}}{\partial\theta}=0. \qquad (18)$$

Relation (18) may be rewritten in an equivalent and rather compact form, as discovered in 2D NMR spectroscopy [3]

$$\vec{\nabla}\Omega_\alpha^{j,n}\times\vec{\nabla}\Omega_\beta^{r,s}=0. \qquad (19)$$

Here Hamilton's nabla operator, $\vec{\nabla}$, is used for the gradient calculations.

Each transition frequency in Eq. (19) depends on p_{m_S} and q_{m_S} from Eqs. (10) and (11), respectively, so that one can rewrite the Jacobian (18) as

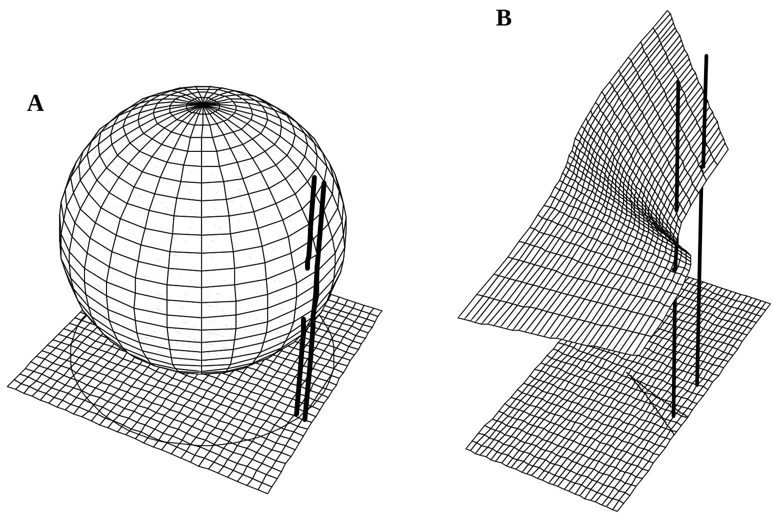

Fig. 2. The two general types of singularities in a smooth mapping $R_2 \Rightarrow R_2$ according to Whitney, (A) a fold which occurs along the circle formed when a sphere is projected onto a plane, and (B) a cusp located at the apex of the triangular figure on the plane. The vertical lines illustrate that (A) points on the plane on opposite sides of the fold correspond to two points of the sphere (the left line crosses the sphere two times) or no points of the sphere (the right line does not cross the sphere); and (B) the number of points projected onto the plane is 3 inside the cusp (the left line crosses the surface three times) and just one outside it (the right line crosses the surface at one point).

$$J = \frac{\partial\Omega_\alpha}{\partial p_\alpha}\frac{\partial\Omega_\beta}{\partial p_\beta}\frac{\partial(p_\alpha,p_\beta)}{\partial(\theta,\phi)} + \frac{\partial\Omega_\alpha}{\partial p_\alpha}\frac{\partial\Omega_\beta}{\partial q_\beta}\frac{\partial(p_\alpha,q_\beta)}{\partial(\theta,\phi)} + \frac{\partial\Omega_\alpha}{\partial q_\alpha} \times \frac{\partial\Omega_\beta}{\partial p_\beta}\frac{\partial(q_\alpha,p_\beta)}{\partial(\theta,\phi)} + \frac{\partial\Omega_\alpha}{\partial q_\alpha}\frac{\partial\Omega_\beta}{\partial q_\beta}\frac{\partial(q_\alpha,q_\beta)}{\partial(\theta,\phi)}. \quad (20)$$

Here the upper indices are omitted for simplicity. The partial derivatives of the transition frequencies in the above equation may be calculated easily using Eq. (15):

$$\frac{\partial\Omega^{j,k}_{m_S}}{\partial p_{m_S}} = \frac{\Omega^{j,k}_{m_S}}{2p_{m_S}} + 2\mathrm{sgn}[k-j]|p_{m_S}|^{1/2}\frac{\partial\xi_{m_S,j+k}}{\partial p_{m_S}}, \quad (21)$$

$$\frac{\partial\Omega^{j,k}_{m_S}}{\partial q_{m_S}} = 2\mathrm{sgn}[k-j]|p_{m_S}|^{1/2}\frac{\partial\xi_{m_S,j+k}}{\partial q_{m_S}}. \quad (22)$$

With the help of Eq. (16) one can obtain

$$\frac{\partial\xi_{m_S,n}}{\partial u_{m_S}} = \frac{1}{3}\cos\left[\frac{\lambda_{m_S}+\pi n}{3}\right]\frac{\partial\lambda_{m_S}}{\partial u_{m_S}}, \quad (23)$$

where u represents p and q as needed. The derivatives of λ may be calculated using its definition in Eq. (9):

$$\frac{\partial\lambda_{m_S}}{\partial p_{m_S}} = \frac{3\cos\lambda_{m_S}}{2p_{m_S}\sin\lambda_{m_S}}, \quad (24)$$

$$\frac{\partial\lambda_{m_S}}{\partial q_{m_S}} = -\frac{\cos\lambda_{m_S}}{q_{m_S}\sin\lambda_{m_S}}. \quad (25)$$

Taking account of Eqs. (8) and (23)–(25) one can rewrite Eqs. (21) and (22) as:

$$\frac{\partial\Omega^{j,k}_{m_S}}{\partial p_{m_S}} = \frac{\Omega^{j,k}_{m_S}}{2p_{m_S}} + \frac{\sqrt{3}\mathrm{sgn}[k-j]\cos\lambda_{m_S}}{4\cos\left[\frac{\pi(k-j)}{3}\right]\sin\lambda_{m_S}}\frac{\Omega_{m_S,j}+\Omega_{m_S,k}}{p_{m_S}}, \quad (26)$$

$$\frac{\partial\Omega^{j,k}_{m_S}}{\partial q_{m_S}} = -\frac{\mathrm{sgn}[k-j]\cos\lambda_{m_S}}{2\sqrt{3}\cos\left[\frac{\pi(k-j)}{3}\right]\sin\lambda_{m_S}}\frac{\Omega_{m_S,j}+\Omega_{m_S,k}}{q_{m_S}}. \quad (27)$$

It is clear that the location of the singularities in the frequency plane can be found by classic mathematical analysis without recourse to catastrophe theory. However, catastrophe theory does allow us to recognize and categorize the types of singularities that do occur. In addition, the ridges of singularities in a spectrum can be quickly visualized with minimal computational effort using another branch of catastrophe theory: the caustics of wave fronts or singularities of the system of rays. When wave fronts, for instance, those of light, propagate through inhomogeneous media, these waves may have high relative amplitude in places because of constructive interference of these waves. That is, at singularities of the wave fronts. Wave front propagation can also be posed in terms of the propagation of rays which are normal to the surface of the wave front. Such a system of rays also may have caustics (singularities) where they are focused by the medium.

On the unit hemisphere, the parallels or lines of latitude start from the pole and expand in a set of concentric circles out to the equator while the meridians or lines of longitude radiate out from the poles, and are everywhere perpendicular to the parallels. These parallels and meridians behave like wavefronts and rays, respectively. The mapping of the unit hemisphere onto the frequency plane by Eq. (17) behaves like the propagation of rays and wavefronts through anisotropic media. The singularities of the mapping occur where rays or wavefronts pile up on top of each other. The prominent singularities in a HYSCORE lineshape can be quickly identified with little computational effort by seeing where the parallels and meridians pile up when they are mapped onto the frequency plane as illustrated later.

Many of our conclusions are based on the mapping of a closed surface onto the frequency plane. Yet the unit hemisphere is not a closed surface and might be expected to have an open 'edge' or boundary. But for magnetic resonance, the unit hemisphere has no bounds from the point of view of topology because of the inversion symmetry of the spin Hamiltonian. The eigenvalues are invariant with respect to inversion of the external magnetic field $\vec{k}_z \Rightarrow -\vec{k}_z$, producing an interesting topological property. The equator of any arbitrary hemisphere is mapped onto the frequency plane twice because the frequencies of opposite points on the sphere coincide. This means that, one can think of the opposite points on the equator as 'glued' together, see Fig. 3, to make the unit hemisphere behave in the context of mapping as if it had no edges. The frequencies change smoothly as one jumps to the opposite point at the equator. Let us underline that the final step after the twofold folding in Fig. 3D is to glue the layers in pairs: the first (counting from top to bottom) with the third, the second with the fourth, this stage is not shown in the figure. Such a glued hemisphere will have self-crossing surfaces. This feature results in rather complex singularity patterns in the general case of the nuclear subhamiltonian having no symmetry and will be illustrated later.

4. HYSCORE spectra in several important cases

We now consider a few general cases of HYSCORE spectra with electron spin $S = 1/2$ and nuclear spin $I = 1$. We discuss some particular cases where special sets of Hamiltonian parameters are imposed by molecular or crystal symmetry. In the most general case, the nuclear subhamiltonian involves nine independent parameters: the nuclear Zeeman frequency, ω_I; the three principal values of the anisotropic hyperfine tensor, $A_{U,U}$ (here U denotes the principal axis direction, $U = X, Y, Z$); the nuclear quadrupolar interaction characterized by its strength κ and asymmetry η; and the three Eulerian angles relating the orientation of the principal axes of NQI tensor to the hfi tensor. This number may by reduced to 8 if the frequency parameters are scaled, e.g., by the nuclear Zeeman frequency. We will comment in Section 5 on the effect of g-factor anisotropy. However, molecular or crystal symmetry may reduce the number of parameters still further, for instance, by making the hyperfine interaction isotropic or the nuclear quadrupole interaction axial.

Catastrophe theory usually deals with the systems of "general position" as explained above. The "general position" situation means that the values of all parameters are not in some way "special," e.g., degeneracy in the energy levels is not allowed. However, in this section we shall consider cases when the nuclear subhamiltonian has non-accidental degeneracies or symmetry so the "general position" condition is not met. In such cases, we will not break the degeneracy or symmetry as usually done in applications of Catastrophe Theory by an arbitrarily small adjustment to the nuclear spin Hamiltonian. Rather, Catastrophe Theory guides us in reducing the angular space that we map so that the degeneracy is removed and we are in a "general position." For example we might map a single octant with a specially chosen orientation instead of mapping the entire hemisphere with an arbitrarily chosen pole and be confident that we have not missed any spectral features.

4.1. Absence of NQI

When the quadrupolar interaction is absent, the three eigenvalues of the nuclear subhamiltonian in each electron spin manifold become equidistant. Due to the coincidence of two transition frequencies the total number of unique

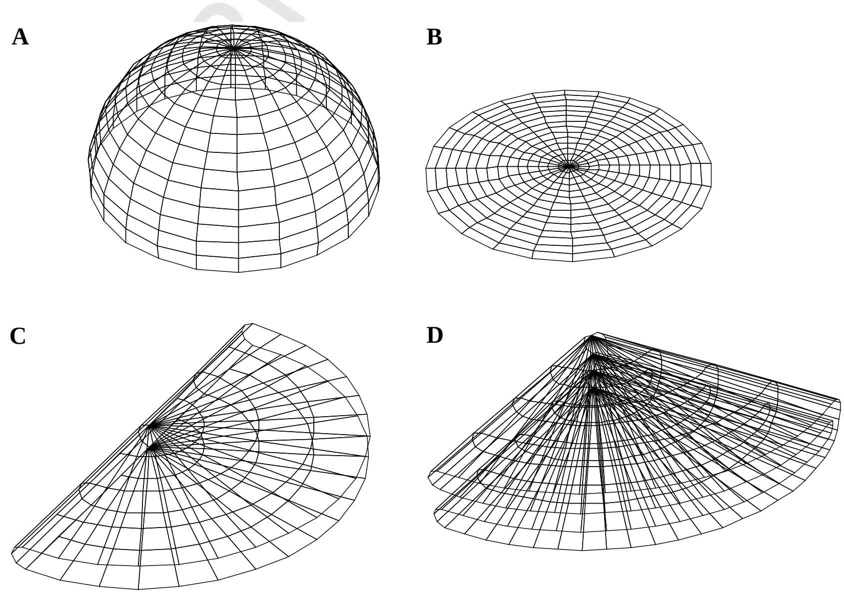

Fig. 3. The topology of the hemisphere due to the symmetry with respect to the inversion. The hemisphere with arbitrary chosen pole as is (A), the hemisphere smoothed out on a plane (B), once (C), and twice (D) folded. After the latter procedure the edges should be glued, the first with the third, and the second with the forth, joining the points where the eigenfrequencies of the nuclear Hamiltonian are the same.

ridges is 16 (in the upper half of the frequency plane) instead of 36 in the general case. The form of the ridges resembles that for nuclear spin $I = 1/2$ discussed in [5]. Here we consider the specific details for spin $I = 1$, giving the Catastrophe Theory results a more conventional explanation.

4.1.1. General case of an anisotropic hyperfine interaction

When the NQI is negligible, the eigenvalues of the nuclear subhamiltonians and respective transition frequencies are easily calculated and the mapping (17) of the singularities onto the frequency plane is simple. The nuclear transition frequencies in this case are calculated from a simplified Eq. (15)

$$\Omega^{j,k}_{m_S} = c_{j,k} D_{m_S}, \tag{28}$$

where $c_{j,k}$ is a constant

$$c_{j,k} = 2\,\mathrm{sgn}(k-j)\sin\left\{\frac{\pi}{6}[1+2(j+k)]\right\} \tag{29}$$

and D_{m_S}, Eq. (12), is the strength (in units of angular frequency) of the effective magnetic field affecting the nucleus in the m_S electron spin manifold,

$$D^2_{m_S} = \omega_I^2 + \frac{1}{4}\vec{k}_z \overleftrightarrow{A}^{\mathrm{T}} \overleftrightarrow{A}\vec{k}_z + m_S\omega_I\vec{k}_z(\overleftrightarrow{A} + \overleftrightarrow{A}^{\mathrm{T}})\vec{k}_z. \tag{30}$$

Here the superscript T denotes the transpose of a matrix. It is clear that $|c_{j,k}| = 2$ for double quantum (dq) nuclear transitions (when $j + k = 1$) or 1 for the single quantum (sq) transitions (when $j + k > 1$). In the principal axis system of the hfi tensor Eq. (30) may be presented as

$$D^2_{m_S} = D^2_{m_S,X}\sin^2\theta\cos^2\phi + D^2_{m_S,Y}\sin^2\theta\sin^2\phi + D^2_{m_S,Z}\cos^2\theta. \tag{31}$$

Here $D_{m_S,U}$ is the length of the vector $\vec{D}_{m_S}$ when the external magnetic field is directed along U-th principal axis of the hfi tensor ($U = X, Y, Z$)

$$D^2_{m_S,U} = \omega_I^2 + \frac{1}{4}A^2_{U,U} + 2m_S\omega_I A_{U,U} \tag{32}$$

with $A_{U,U}$ being a principal value of the hfi tensor. First we consider the case when all these values are different. Axial symmetry of the hfi tensor is considered below as a special case.

In the absence of NQI, additional symmetry features appear in the mapping (17). The substitutions $\phi \Rightarrow 2\pi - \phi$ and $\phi \Rightarrow \pi \pm \phi$ (in the system of hfi tensor) lead to the same transition frequencies (28). It means that the hemisphere is mapped four times onto the same ridges in the frequency plane and that the mappings of its four octants coincide. In this case the hemisphere (for the sake of discussion, the upper one, where $\cos\theta \geqslant 0$) is folded in half twice, causing pairs of folds to coincide. Such degeneracy violates the "general position" situation considered by catastrophe theory. To resolve this situation, we cut one octant out of the whole sphere first along the edges $\phi = 0$ and $\phi = \pi/2$, and then along the equator where $\theta = \pi/2$ (see Fig. 3, giving one of the four layers in D). The 'edges' map onto the frequency plane as a set of fold singularities. These folds may also be obtained as formal solutions of Eq. (18) or the more complex relation, Eq. (20). Eq. (18) takes a simple form that will be seen later

$$J \propto \Psi(\theta,\phi) = \cos\theta\sin^3\theta\cos\phi\sin\phi = 0, \tag{33}$$

which gives the same folds obtained from our consideration of the symmetry of the transition frequencies.

The mappings of the folds—the two meridians $\phi = 0$, $\phi = \pi/2$ and the equator $\theta = \pi/2$—form the boundaries of the HYSCORE line in the frequency plane, which is the mapping of the spherical triangle. The shape of the HYSCORE line is a curvilinear triangle and it is possible to find analytical relations for its boundaries in the frequency plane. The ridges are simple triangles when considered in terms of squares of the two frequencies, (ω_1^2, ω_2^2), called the ω^2-plane for simplicity. For the fold along the equator, $\cos\theta = 0$, so that one obtains a parametric form for Eq. (17):

$$\begin{aligned} \omega_1^2 &= c^2_{j,n}\left[D^2_{\alpha,X} + (D^2_{\alpha,Y} - D^2_{\alpha,X})\sin^2\phi\right], \\ \omega_2^2 &= c^2_{r,s}\left[D^2_{\beta,X} + (D^2_{\beta,Y} - D^2_{\beta,X})\sin^2\phi\right], \end{aligned} \tag{34}$$

which is a straight line segment on the ω^2-plane connecting the points $(c^2_{j,n}D^2_{\alpha,X}, c^2_{r,s}D^2_{\beta,X})$ and $(c^2_{j,n}D^2_{\alpha,Y}, c^2_{r,s}D^2_{\beta,Y})$. The two other folds also map as straight line segments which connect these two points with the map of the pole at $(c^2_{j,n}D^2_{\alpha,Z}, c^2_{r,s}D^2_{\beta,Z})$. Examples of ridges in the absence of NQI are displayed in Fig. 4. The standard frequency plane and the ω^2-plane are shown. The only singularities are the folds which outline each of the HYSCORE lines.

The signal intensity is exactly zero when the external magnetic field lies along a principal axis of the hyperfine tensor. This condition occurs at the vertices of each ridge in the HYSCORE spectrum for this nuclear spin Hamiltonian. Thus, the singularities can be prominent on the sides of each HYSCORE line, but must vanish at the vertices. However, the vertices can be easily located by a simple linear extrapolation of the singularity edges in the ω^2-plane [5]. The vertices give the frequencies of the principal values of the hfi and therefore completely describe the hfi and the nuclear spin subhamiltonians.

Both single quantum transition frequencies are the same for this nuclear spin Hamiltonian which imparts a characteristic feature to the HYSCORE spectrum that has some utility in the analysis of spectra. The sq–dq and dq–sq ridges have the same form of the sq–sq ridges but are expanded by a factor of two in one dimension, and the dq–dq ridges are expanded in both dimensions. If point (ω_1, ω_2) is observed on a sq-sq singularity on the frequency plane, the following points also lie on singularities and have nonzero spectral density: sq–dq—$(\omega_1, 2\omega_2)$, dq–sq—$(2\omega_1, \omega_2)$, dq–dq—$(2\omega_1, 2\omega_2)$, and due to the symmetry features of the HYSCORE spectra, (ω_2, ω_1), $(\omega_2, 2\omega_1)$, $(2\omega_2, \omega_1)$, $(2\omega_2, 2\omega_1)$. In addition, all the HYSCORE lineshapes are simple triangles in the ω^2-plane.

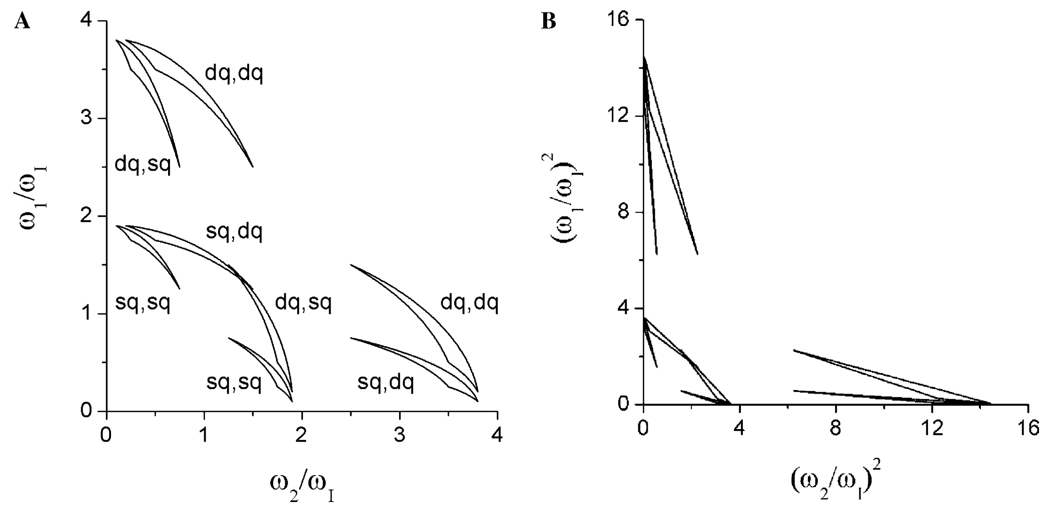

Fig. 4. The singularities of the HYSCORE spectrum in the absences of NQI (A) on the frequency plane, the types of correlation are indicated for each HYSCORE line; and (B) on the ω^2-plane. Parameters of the nuclear subhamiltonian were as follows: $\omega_I = 1$, $A_{X,X} = 1.8$, $A_{Y,Y} = 0.5$, and $A_{Z,Z} = 1.5$.

These results systematically extend our earlier results [5] from $I = 1/2$ to arbitrary I in the absence of NQI. We note here that Eq. (28) is quite general for all I when $\kappa = 0$, with $c_{j,k}$ taking integer values from 1 to $2I$, so that all HYSCORE lines, whether involving single or multiple quanta, have the same shape properties as for $I = 1$ and that the only singularities are the folds outlining each HYSCORE line.

4.1.2. Axial symmetry of the hyperfine interaction

The case of axial symmetry of the hfi tensor introduces additional degeneracies because two principal values of this tensor coincide. This leads to significant simplification of Eq. (31)

$$D^2_{m_S} = D^2_{m_S,\parallel}\cos^2\theta + D^2_{m_S,\perp}\sin^2\theta, \tag{35}$$

where $D_{m_S,\parallel}$ and $D_{m_S,\perp}$ are just redefinitions of the quantities given in Eq. (32).

In this situation, the transition frequencies are independent of the azimuth angle ϕ, so that the Jacobian (18) vanishes on the whole sphere

$$J_{\mathrm{axial}}(\kappa = 0) \equiv 0. \tag{36}$$

This means that all HYSCORE lines have zero width, and the triangles in the ω^2-plane collapse to straight line segments because two vertexes of triangle coincide (the equator is mapped onto a single point in this case). "General position" is met by every chord connecting the pole and the equator. The ridges become curvilinear segments in the standard frequency plane with delta function cross sections and straight line segments in the ω^2-plane which completely describe the hfi [5]. These results hold for all values of $I \geqslant 1$ and for crosspeaks of all possible quantum orders.

4.2. Arbitrary NQI

Addition of a quadrupole interaction removes the degeneracy of the single quantum transition frequencies for nuclear subhamiltonians except in a few very special situations described below. There are potentially 36 ridges in the frequency plane, but some of these ridges may overlap. We do not consider the case of an axially symmetric quadrupolar interaction separately because it is obtained naturally in the limit of small asymmetry.

4.2.1. Isotropic hyperfine interaction

Systems having arbitrary NQI and isotropic hyperfine interaction were considered earlier in detail [16]. It was shown that the HYSCORE lines have zero width, because the effective field affecting the nuclear spin, Eq. (12), is directed along the external magnetic field for both electron spin manifolds. In such a situation, the parameters p_{m_S} (see Eq. (10)) are independent of the PC orientation and the parameters q_{m_S} depend on the same function of orientation, $f(\eta, \theta, \phi)$, [15,16] for both manifolds. The immediate consequence is that the Jacobian (18) vanishes

$$J_{\mathrm{iso}}(\kappa \neq 0) \equiv 0. \tag{37}$$

There is no simple way to transform the curvilinear zero width ridges into straight line segments (as could be done in the absence of NQI) or even into simple polynomial or trigonometric functions.

4.2.2. Coincident principal axes for NQI and hfi

When the NQI and hfi principal axes coincide, the quantities p_{m_S} and q_{m_S} in Eqs. (10) and (11) may be arranged in the form of Eq. (31), for example:

$$\begin{aligned} q_{m_S} &= q_{m_S,X}\sin^2\theta\cos^2\phi + q_{m_S,Y}\sin^2\theta\sin^2\phi + q_{m_S,Z}\cos^2\theta, \\ p_{m_S} &= p_{m_S,X}\sin^2\theta\cos^2\phi + p_{m_S,Y}\sin^2\theta\sin^2\phi + p_{m_S,Z}\cos^2\theta, \end{aligned} \tag{38}$$

where θ and ϕ define the direction of the external magnetic field in the principal axis system of both tensors, and

$$q_{m_S,U} = Q_{U,U}\left\{\omega_I^2 + \frac{1}{4}A_{U,U}^2 + 2m_S\omega_I A_{U,U}\right\} - 2\kappa^3(1-\eta^2),$$
$$p_{m_S,U} = -\left[\omega_I^2 + \frac{1}{4}A_{U,U}^2 + 2m_S\omega_I A_{U,U} + \kappa^2(3+\eta^2)\right]. \tag{39}$$

Here $Q_{U,U}$ are the principal values of the NQI tensor ($U = X, Y, Z$) given in Eq. (13).

The nuclear transition frequencies in this case depend on the orientation of the external magnetic field in a rather complex manner, yet they possess the same symmetry features as described above in the absence of NQI. This means that the mappings of the four octants of the hemisphere onto the frequency plane coincide, that "general position" can be achieved by the same reduction of the unit hemisphere to an octant, and that Eq. (33) is still valid for the singularities of the mapping.

However, additional singularities are now possible. Eq. (20) can be factored so that the four components of the Jacobian may be calculated as the product of two terms:

$$\begin{aligned} J = 4\Psi(\theta,\phi) \times \bigg[&\frac{\partial\Omega_\alpha}{\partial p_\alpha}\frac{\partial\Omega_\beta}{\partial p_\beta}\{p_{\alpha,Y}p_{\beta,Z} - p_{\alpha,Z}p_{\beta,Y} + p_{\alpha,Z}p_{\beta,X} \\ &- p_{\alpha,X}p_{\beta,Z} + p_{\alpha,X}p_{\beta,Y} - p_{\alpha,Y}p_{\beta,X}\} + \frac{\partial\Omega_\alpha}{\partial q_\alpha}\frac{\partial\Omega_\beta}{\partial p_\beta} \\ &\times\{q_{\alpha,Y}p_{\beta,Z} - q_{\alpha,Z}p_{\beta,Y} + q_{\alpha,Z}p_{\beta,X} - q_{\alpha,X}p_{\beta,Z} \\ &+ q_{\alpha,X}p_{\beta,Y} - q_{\alpha,Y}p_{\beta,X}\} + \frac{\partial\Omega_\alpha}{\partial p_\alpha}\frac{\partial\Omega_\beta}{\partial q_\beta}\{p_{\alpha,Y}q_{\beta,Z} - p_{\alpha,Z}q_{\beta,Y} \\ &+ p_{\alpha,Z}q_{\beta,X} - p_{\alpha,X}q_{\beta,Z} + p_{\alpha,X}q_{\beta,Y} - p_{\alpha,Y}q_{\beta,X}\} \\ &+ \frac{\partial\Omega_\alpha}{\partial q_\alpha}\frac{\partial\Omega_\beta}{\partial q_\beta}\{q_{\alpha,Y}q_{\beta,Z} - q_{\alpha,Z}q_{\beta,Y} + q_{\alpha,Z}q_{\beta,X} - q_{\alpha,X}q_{\beta,Z} \\ &+ q_{\alpha,X}q_{\beta,Y} - q_{\alpha,Y}q_{\beta,X}\}\bigg]. \end{aligned} \tag{40}$$

Singularities arise in the mapping (17) if either term in the product vanishes. The first term on the right hand side is $\Psi(\theta,\phi)$ from Eq. (33), and results from the symmetry produced by coincident principal axes. The second factor, in square brackets, may be rewritten in compact form as

$$\sum_{u,u'=p,q}\frac{\partial\Omega_\alpha}{\partial u_\alpha}\frac{\partial\Omega_\beta}{\partial u'_\beta}(\vec{a}\cdot(\vec{u}_\alpha\times\vec{u}'_\beta)) = 0. \tag{41}$$

Here, the auxiliary vectors, $\vec{p}_{m_S} = (p_{m_S,X}, p_{m_S,Y}, p_{m_S,Z})$, $\vec{q}_{m_S} = (q_{m_S,X}, q_{m_S,Y}, q_{m_S,Z})$, and $\vec{a} = (1,1,1)$, are introduced. Unfortunately, there seems to be no simple way to solve Eq. (41) except numerically.

Fig. 5 displays some examples of the singularities of the dq, dq HYSCORE line in a frequency spectrum (right-hand side where the singularities appear as folds or turning points of the projected surfaces in the frequency plane) and the respective lines where $J = 0$ on a 'flattened' unit hemisphere (left-hand side) for different values of the quadrupole coupling constant. These two displays are complementary with the frequency display showing the frequencies of the singularities, but not the corresponding orientations; while the hemisphere display shows the orientations where the singularities occur but not their frequencies. The parameters were chosen to show a range of features in the patterns.

The singularities are shown as solid lines in both types of displays. The patterns look like projections of curvilinear triangles whose edges are defined by $\Psi(\theta,\phi) = 0$ in Eq. (33). These 'triangles' may appear twisted and possess additional singularities if additional folds appear from Eq. (41). These additional singularities are better resolved on the surface of the hemisphere than on the frequency plane. There are two types, the first looks like a bubble connected to one edge of the octant (Fig. 5D) while the second connects two different sides of the octant (cases B, E, and F). These additional folds are too close to the folds from Eq. (33) to be resolved in the frequency plane.

The HYSCORE line in Fig. 5C has a heel-like pattern on the lower, right-hand side which becomes a narrow spike in Fig. 5D when the bubble at the equator of the hemisphere appears. The width of the spike approaches zero as the bubble approaches the meridian with coordinates $\theta = \phi = \pi/2$ (where it is highly degenerate, and is not shown in Fig. 5 because it is not a 'general position'). When κ exceeds some critical value ($\sim$0.61 for the current parameters), the pattern becomes like that in Fig. 5E and looks like a twisted triangle in the frequency plane.

Fig. 6 illustrates other features of additional folds in the frequency plane. In Fig. 6A the distance between the additional fold (the mapping of a curvilinear segment near the pole from the left part of Fig. 5B) and the mappings of both meridians, $\phi = 0$ and $\phi = \pi/2$, are displayed. The mappings of the meridians cross each other. The triangle at the right part of Fig. 5B is twisted near its leftmost vertex. The distance does not exceed $10^{-3}\ \omega_I$ and will produce an intense and likely unresolvable peak. Fig. 6B shows the additional fold in Fig. 5D and the main fold, which is a mapping of the equator. The distance between these features is less than $10^{-4}\ \omega_I$, meaning that the entire surface area of the bubble on the left-hand side of Fig. 5D is mapped onto a very narrow strip in the frequency plane, producing an unresolved region of high spectral density.

In the frequency plane, these additional folds resemble caustics of a system of rays or wave fronts (shown as dashed lines in the figure), e.g., the right-most edge in Fig. 5F.

There is an important and useful feature of these HYSCORE patterns that can aid in the interpretation of spectra. The positions on the hemisphere which are solutions of Eq. (33) depend neither on the transition number nor on the electron spin manifold when the tensor axes are coincident. Along the edges of the octants defined by the coincident principal axes of the NQI and hfi, all three transitions of each manifold map to fold singularities. If a vertical (or horizontal) line is drawn through the HYSCORE spectrum so that it intersects the ridges for all three nuclear transitions (as shown in Fig. 7), that ver-

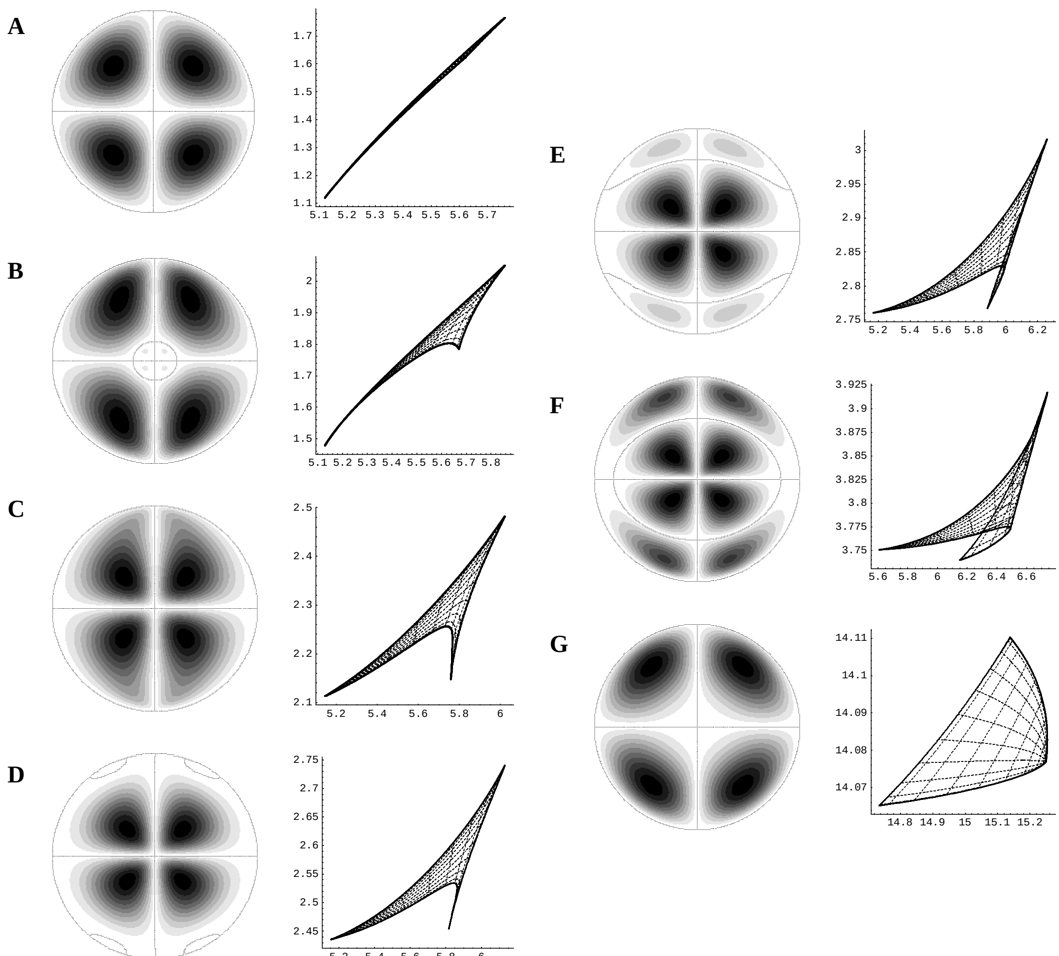

Fig. 5. The value of $|J|/\sin\theta$ on the hemisphere surface (with solid line drawn for orientations where the Jacobian $J = 0$) (first column) and that of the singularities on the frequency plane of dq–dq ridge (second column). The radius is proportional to the value of angle θ, $0 \leqslant \theta \leqslant \pi/2$. The quadrupole coupling constant was varied, $\kappa = 0.04$ (A), 0.3 (B), 0.5 (C), 0.6 (D), 0.7 (E), 1.0 (F), 4.0 (G), from top to bottom. All other parameters were as follows, $\omega_I = 1$, $\eta = 0.5$, $A_{X,X} = 3.76$, $A_{Y,Y} = 3.62$, and $A_{Z,Z} = 3.12$.

tical line intersects the singularity lines of Eq. (33) at frequencies related by

$$\Omega^{0,1}_{m_S} = \Omega^{1,2}_{m_S} + \Omega^{2,0}_{m_S}. \tag{42}$$

This general relation is useful for interpreting HYSCORE ridges and for relating them back to the orientation of the molecule. The positions of singularities given by the solutions of Eq. (41) that are not octant edges, do not have this property because those singularities correspond to different orientations with different sets of frequencies for each HYSCORE line. The frequencies along the octant edges can be used to determine elements of Eqs. (38) and (39).

In the case of weak quadrupole interaction, relation (42) for the singularities is a good approximation even when the tensor principal axes do not coincide, thus allowing fairly accurate estimation of the spin Hamiltonian parameters.

4.2.3. The absence of any symmetry

When the principal axes of NQI and hfi are not collinear, there are no elements of additional symmetry in the nuclear spin Hamiltonian (7) to aid in solving the right-hand side of Eq. (20) and numerical methods are required.

The quantities p_{m_S} and q_{m_S} are defined in terms of the invariants [16] of the Hamiltonian and depend quadratically on components of the unit vector $\vec{k}_z$. The quantity $-p_{m_S}$ is positively defined which, in principle, allows one to diagonalize both terms by the same linear transformation [19]. Unfortunately, this transformation is not a simple rotation of the coordinate system; a rescaling of the spatial axes is also required. Consequently, the unit sphere is transformed into a three-axis ellipsoid in a new system of coordinates. Moreover, the transformations are different for the each electron spin manifold, limiting the usefulness of these transformations in solving the equation $J = 0$ to find the singularities.

Fortunately, it is not necessary to find the zeroes of Eq. (40) to locate the singularities in the frequency plane. At the end of Section 3, we described a method from Catastrophe Theory to visualize the singularities simply by projecting the parallels and meridians of an arbitrarily oriented unit hemisphere onto the frequency plane. Fig. 8 shows a

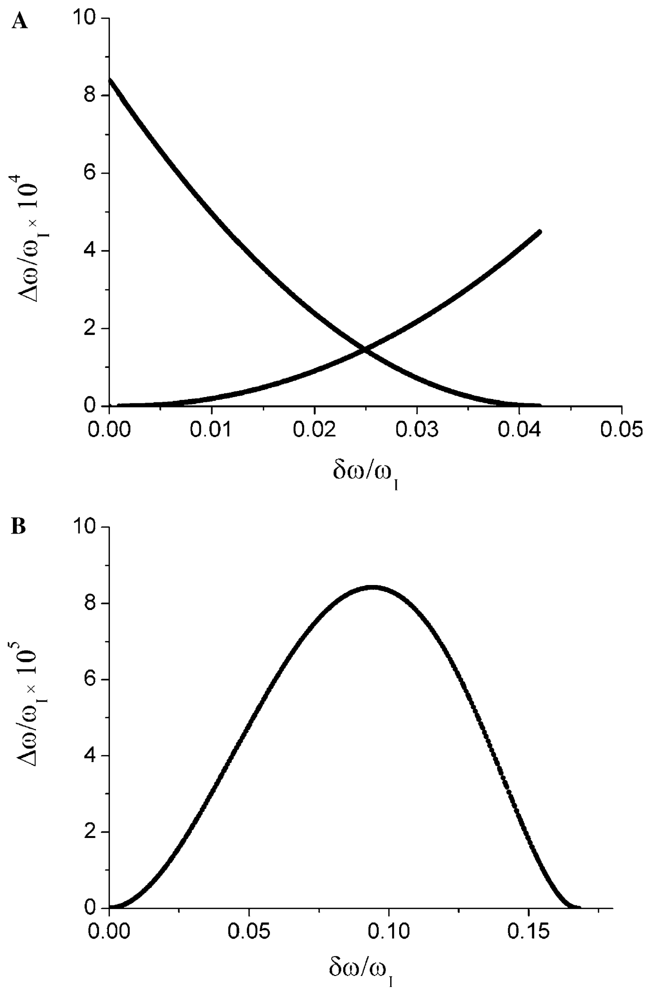

Fig. 6. The distance between additional singularity lines and sides of curvilinear triangles. (A) Additional singularity from Fig. 5B. The distances between mapping of the arc near the pole and mappings of the meridians ($\phi = 0$ and $\phi = \pi/2$) on the frequency plane ($\Delta\omega$) is plotted versus the distance at the frequency plane between the mappings of the crossing point of the arc and the meridian $\phi = 0$ and that of the point of the arc ($\delta\omega$). (B) Additional singularity from Fig. 5D. The distance between the mapping of the edge of the 'bubble' and the mapping of the equator ($\Delta\omega$) is plotted versus the distance between the mappings of the crossing point of the bubble and equator and the mapping of point of the bubble ($\delta\omega$).

set of maps of the parallels and meridians of the unit hemisphere onto the frequency plane illustrating this method. The folds are easily recognized from the abrupt change in contrast although the internal cusps are not always apparent when the figures are drawn at low resolution with a limited number of parallels and meridians.

This method of visualizing the singularities is fast and efficient because it only requires calculating the eigenvalues for the mapping of Eq. (17) and does not require the intensity coefficients for Eq. (14) or the Jacobian in Eq. (40) or its roots. It can be useful for rapidly exploring parameter space of any spin Hamiltonian to find an initial match between singularities and the prominent features in an experimental spectrum before investing in more time-consuming simulations.

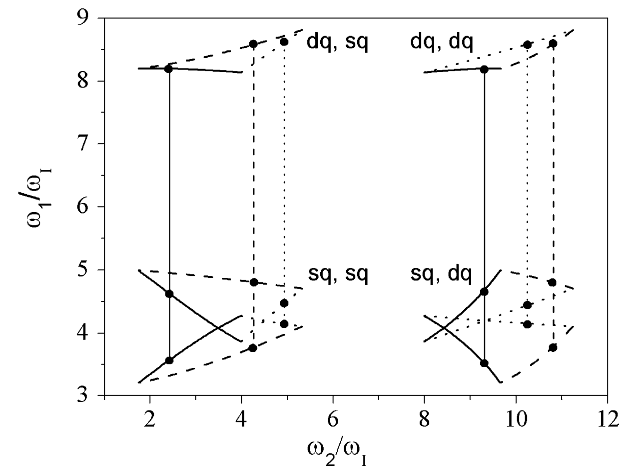

Fig. 7. Example of the additive relation of Eq. (42) between singularities from Eq. (33). Three ridges of $m_S = -1/2$ manifold correlate the double quantum transition (right 'column') and one of the single quantum transitions (left 'column') of $m_S = 1/2$ electron spin manifold. Parameters are as follows, $\omega_I = 1$, $\kappa = 2$, $\eta = 0.9$, $A_{X,X} = 6.1$, $A_{Y,Y} = 4.7$, and $A_{Z,Z} = -0.3$. The type of line dashing is the same for the same folds. The vertical lines illustrate that points on the same 'edge' (marked by the solid dots) are related by Eq. (42). This relationship can be used to distinguish Eq. (33) singularities from those of Eq. (41) and to identify which singularities correspond to the same 'edge.'

There are several important characteristics for this case of no symmetry. One is that none of the singularities necessarily correspond to principal values of the hfi or NQI tesnors, or even to θ or ϕ taking on values of 0 or $\pi/2$. Consequently, it can be dangerous to interpret features in the spectrum as principal values. A second characteristic is that the singularities for each HYSCORE line with different n_α and n_β can occur at different orientations on the unit hemisphere. That is, plots like those on the left-hand side of Fig. 5 can be different for each of the nine 'unique' HYSCORE lines. As a consequence, singularities in two different lines generally correspond to two different orientations and the additive relation in Eq. (42) and Fig. 7 will not hold. A final characteristic is that the internal singularities, for a variety of reasons, can be more intense in a spectrum than the fold that outlines the HYSCORE line. As a consequence, the observed features in a spectrum can not be considered as an upper or lower bound for that transition.

5. General features of HYSCORE spectra

Every HYSCORE line in spectra from a collection of randomly oriented PCs has certain common features. The most important feature is that the outer edge of each ridge is a singularity line. This property results from the fact that the frequencies are analytic functions of the orientation and are degenerate with respect to inversion of the magnetic field.

This is easily seen in Fig. 8 where the unit hemisphere maps onto the frequency plane as one continuous closed surface. Because the surface has no 'edges', the boundaries

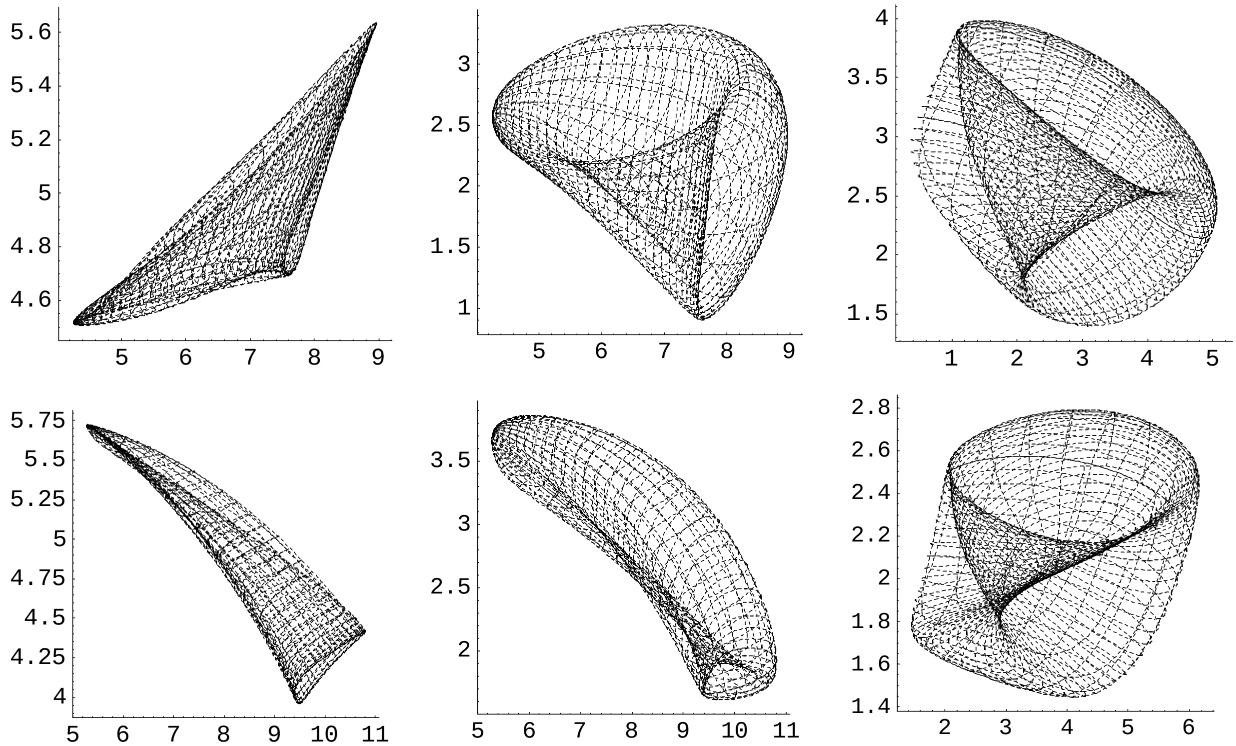

Fig. 8. Fast visualization of the singularity ridges by mapping the parallels and the meridians from the hemisphere onto the frequency plane. Parameter values for the upper row were as follows: $\omega_I = 1$, $\kappa = 2$, $\eta = 0.9$, $A_{X,X} = 6.1$, $A_{Y,Y} = 4.7$, $A_{Z,Z} = -0.3$, Euler angles (orientation of the NQI tensor system with respect to the hfi principle axes) were 50°, 40°, and 80°, for the lower row the nuclear Zeeman frequency was a factor of two larger, $\omega_I = 2$. The ridges correlating transitions with $n_\alpha = n_\beta = 1$ (dq, dq) (the first column); $n_\alpha = 1$, $n_\beta = 2$ (dq, sq) (the second column); and $n_\alpha = 2$, $n_\beta = 3$ (sq, sq) (the third column) are displayed. The (dq, dq) transitions for both sets of parameters resemble the 'glued' hemisphere in Fig. 3D. Each of the three sides has two crossing folds. Conversely, the (dq, sq) and (sq, sq) lines are bounded by a single fold but have an additional set of internal singularities that appear to be threefold joined at three cusps.

of the HYSCORE line must be a fold and hence a singularity. Consequently, the boundaries or 'contour lineshape' [5] is a significant feature of HYSCORE spectra for nuclei with any spin. When the NQI is significant, there may be other singularities on the interior of a HYSCORE line and some care is needed that they are not mistaken for the boundary of the line.

The singularities in HYSCORE spectra are modified by experimental conditions in three ways. (1) The singularities are not infinite in intensity, but become sharp ridges because of the finite range of the observation times t_1 and t_2, [5], broadening from electron and nuclear spin relaxation and from 'strain' or a dispersion in the NQI or hfi parameters. (2) This paper focuses on the singularities caused by mapping. The intensity factors, A and B, Eq. (14), can become zero and make a portion of the singularity disappear. Although A and B are functions of τ, Fig. 1B, there can be regions of the unit hemisphere where A and B vanish for all values of τ, making some portion of the singularity unobservable. Fig. 9 shows the singularities (or Fourier transform 'star' artifacts) and the corresponding calculated HYSCORE contour spectra that take into account the intensity factors. All the major features in the calculated spectra corresponds to singularities. This agreement between spectral features and singularities justifies our focus on the singularities at the expense of the intensities which also depend on experimental and data processing parameters. (3) An experimental measurement may not include all of the orientations represented by the unit hemisphere. If the paramagnetic centers in the sample are even partially ordered, some regions of the unit hemisphere will not be represented in the measurement and singularities in those un- or under-represented regions will be absent or reduced. In similar fashion, the EPR resonance condition may prevent some orientations of the paramagnetic center from participating in the HYSCORE measurement, a condition known as 'orientation selection' and is often the result of large g-factor anisotropy. The probability, $P(\theta,\phi)$, that an orientation contributes to the spectrum enters into the integration over the unit hemisphere to obtain the HYSCORE spectrum in either the time- or frequency-domain. The integral can be rearranged to incorporate P with the intensity factors A and B. It then is possible to write Eq. (14) with $A'_{njrs}(\theta,\phi) = P(\theta,\phi)A_{njrs}(\theta,\phi)$, and similarly for the B term, replacing the original A and B. The A' and B' are still bounded because the normalized P are also bounded. Thus, we make the same arguments made earlier that the prominent features in an experimental HYSCORE spectrum will coincide with singularities. However, there may be fewer features because the orientations that give rise to them are absent from the observation.

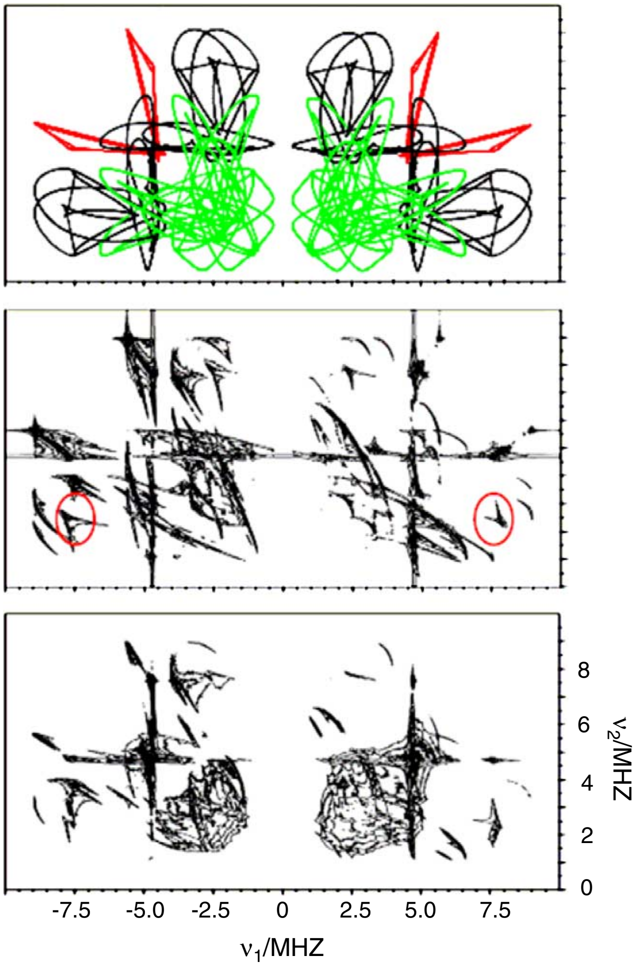

Fig. 9. Singularities for all possible crosspeaks and HYSCORE spectra simulated using the program HYSCORE3 by A.M. Tyryshkin. The upper figure are the singularities: red denotes the dq, dq singularities; black the dq, sq and sq, dq; and green the sq, sq. The middle figure is a simulated spectrum in the limit of small τ (=10 ns) and the lower spectrum is simulated with $\tau = 200$ ns. Spectra were simulated in the time domain from $t_1 = t_2 = 0$ and processed without apodization. Parameter values are: $\omega_I = 1$, $\kappa = 2$, $\eta = 0.9$, $A_{X,X} = 6.1$, $A_{Y,Y} = 4.7$, $A_{Z,Z} = -0.3$, Euler angles (orientation of the NQI tensor system with respect to the hfi principle axes) are 50°, 40°, and 80° for $g = 2.0023$ with $S = 1/2$, $I = 1$. The red ellipses in the middle figure mark internal fold singularities meeting in cusps for the dq, sq and sq, dq lines. The three figures are plotted to the same frequency scale.

The orientational probability, P, is under some experimental control, for example, by changing the resonance condition when there is orientation selection or by rotating the samples when there is partial alignment. There may be some possibility of extracting information about P from a series of HYSCORE spectra, but our interest is focused on the ability to use the singularities to make a rapid analysis of hfi and NQI parameters. Even in the presence of g-factor anisotropy, it still is feasible to exploit the mapping singularities with a set of experimental spectra obtained at several positions in the anisotropic EPR spectrum.

The singularities in the HYSCORE lines change smoothly as the nuclear Zeeman, hfi, and NQI parameters vary because the transition frequencies of the nuclear subhamiltonian involved in the mapping are analytic functions of these parameters. Eight dimensionless parameters describe the nuclear subhamiltonian, which are too many to study systematically in a single paper. Only one parameter, the nuclear Zeeman interaction, is an experimental variable, it depends on the EPR measurement frequency through the EPR resonance condition. Recent progress in pulsed EPR instrumentation suggest that it may soon be possible to make HYSCORE measurements for some nuclei with EPR frequencies in the range of 0.3–270 GHz. We show, Fig. 10, a few examples of HYSCORE lineshapes in this frequency range. We use preliminary hfi and NQI parameters for one of the nitrogens in the Rieske iron–sulfur cluster with the tensor axes slightly skewed and we completely ignore orientation selection. This example does not correspond to any of the special cases discussed above and most of the calculated lines contain internal singularities.

There are three types of HYSCORE lines, each with its own properties. The dq, dq lines ($n = j + k = 1$ in Eq. (15)) start at low EPR frequencies as narrow lines, roughly parallel to the diagonal of the frequency plane. The dq, dq lines broaden and then narrow as EPR frequency increases, becoming narrow ridges roughly perpendicular to the diagonal in the high frequency limit. At low frequency, the transition frequencies for the two transitions are nearly degenerate, producing a line on the diagonal. At high frequencies, the NQI is a slight perturbation on the dq frequencies and the lineshape converges to that for vanishing NQI.

For the sq, sq line with $n = 2$ (or 3) for both frequencies, the lineshape is again a straight line along the diagonal at low frequency for the same reason as for the dq, dq transition. The line broadens with increasing frequency, reaching a limiting shape when $\omega_I \gg$ hfi determined by both the hfi and NQI. This high frequency limit may provide good conditions for complete determination of the spin Hamiltonian parameters because the shapes approach the 'first-order' lineshape.

Lines characterized by different values of n (the dq, sq and some sq, sq lines) are generally broad at all frequencies because the anisotropy of the two transition frequencies involved are generally quite different for finite NQI. The strongest changes of the HYSCORE patterns take place when the nuclear Zeeman frequency has the value close to the cancellation condition, $\omega_I = 1/2a$ (K-band for the parameter set at Fig. 10) [20].

The intensity factors, A and B, vary with the inverse square (or even higher power) of the EPR frequency at high frequency, placing a practical limit on high frequency measurements. However, the high sensitivity and first-order lineshapes may make high-frequency measurements desirable. For finite NQI, the intensities reach a limiting, generally non-zero, value for low EPR frequencies because the eigenfunctions in the two electron spin manifolds become complex conjugates of each other although the eigenvalues become degenerate [21].

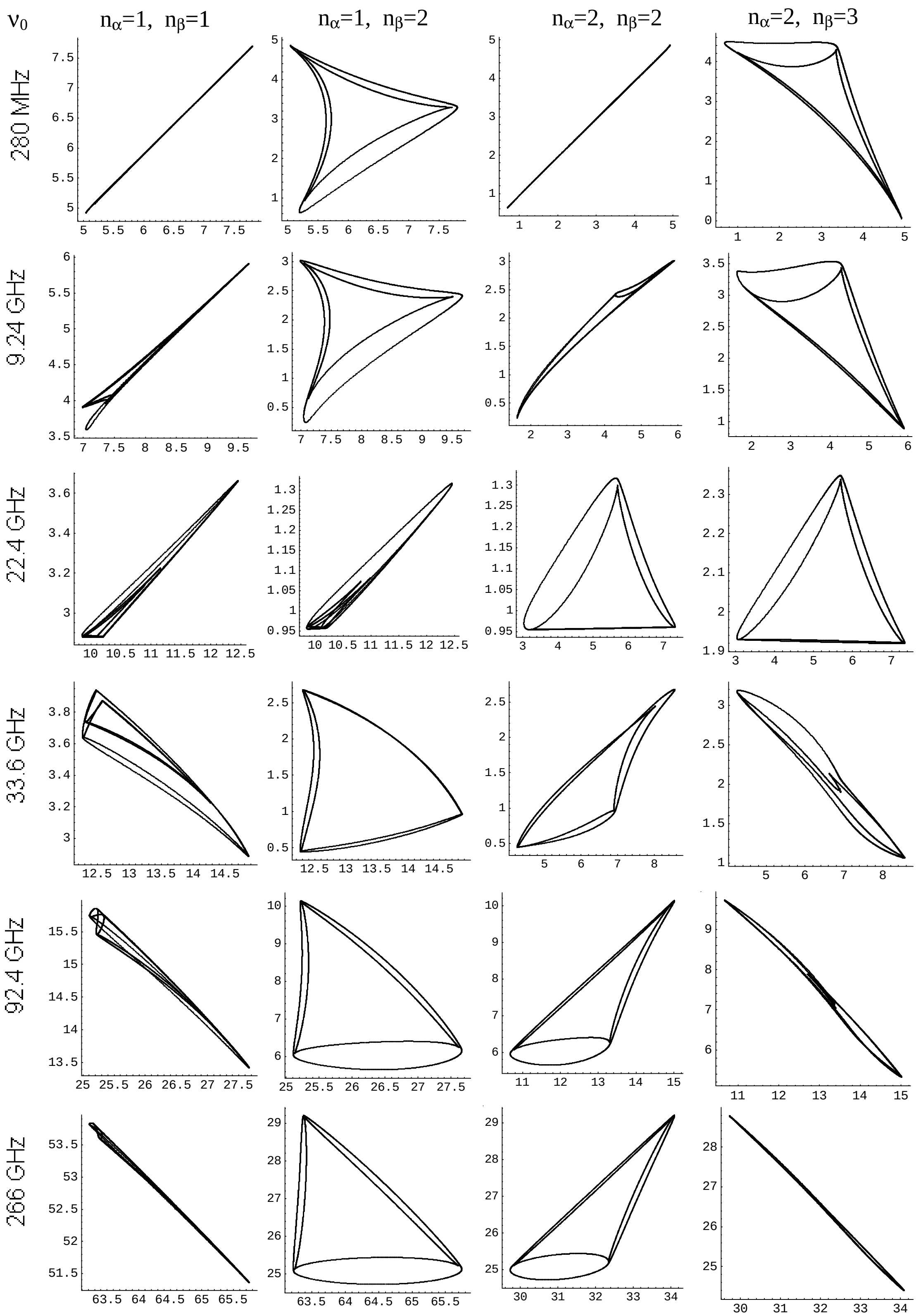

Fig. 10. The example of the transformations of the ridges singularities with variation of the external magnetic field strength for ridges of different types. The types of the ridges are in the column headings. The working frequency of the EPR spectrometer is shown in the leftmost column, the nuclear Zeeman frequency was calculated for ^{14}N nucleus. The other parameters needed for calculations were as follow, $\kappa = 0.8$ MHz, $\eta = 0.6$, $A_{X,X} = 7.2$ MHz, $A_{Y,Y} = 4.7$ MHz, $A_{Z,Z} = 4.9$ MHz, Euler angles (orientation of the NQI tensor system with respect to the hfi principle axes) were 10°, 15°, and 5°.

6. Conclusions

The 2D spectra of disordered systems are, from mathematical point of view, smooth mappings of the hemisphere of possible orientations of the external magnetic field with respect to the molecular frame of the PC. The spectrum consists of 36 ridges on the upper half of the frequency plane. Catastrophe theory explains the positions of the singularities of such mappings and provides a classification of them. In our case of smooth mapping of one 2D space onto the other there can be only two types of singularities: folds and cusps. The major features in experimental spectra appear to correspond to these singularities, although not every singularity is seen in any single experimental spectrum.

The analysis is based on exact solution of the nuclear spin Hamiltonian. Systems with negligible quadrupole interaction have equidistant nuclear eigenvalues for each electron spin manifold and possess additional elements of symmetry. The singularities in this case are mappings of the large arcs connecting the crossing points of the hemisphere with lines directed along the principle axes of the hyperfine interaction tensor. HYSCORE spectra of such systems are curvilinear triangles on the frequency plane and straight line triangles on the ω^2-plane. The sides of those triangles in both representations are singularities of the mapping and the only singularities in this case. The number of unique ridges in the spectrum is reduced to 16 because the frequencies of the two single quantum nuclear transitions are degenerate. When the principle axes of NQI and hfi tensors coincide, the system has the same elements of symmetry as in the absence of NQI and the singularity patterns are curvilinear triangles. There is no simple general function that describes these curvilinear segments. The singularities related to the same transition satisfy relation (42), which may be used for verifying of the coincidence of the systems of the principle axes of NQI and hfi tensors. Additional singularities appear for some values of the Hamiltonian parameters. These may be very close to the sides of triangle thus providing quite large spectral densities. The singularity patterns appear at times like a projection of twisted triangles. In all cases, the bounds of the HYSCORE ridges are singularities of the mapping. There may also be internal singularity lines inside each ridge and singularity lines may cross on the frequency plane.

The singularity patterns are strongly dependent on the operating frequency of the pulsed EPR spectrometer. The most significant transformations take place when the nuclear Zeeman frequency becomes approximately equal to the half of the isotropic hyperfine constant (cancellation condition).

Analysis of singularity patterns is simpler and needs less time than calculations of the HYSCORE signal intensities and provides a promising means for preliminary estimations of the spin Hamiltonian parameters.

Acknowledgments

This work was supported by the National Institutes of Health, GM61904 and partly by Russian Grant for Scientific Schools, 919.2003.3. A.G.M. thanks Battelle Memorial Institute for a Visiting Scientist Fellowship. Part of this work was performed at the WR Wiley Environmental Molecular Sciences Laboratory, a National Scientific User facility sponsored by the Department of Energy's Office of Biological and Environmental Research and located at Pacific Northwest National Laboratory. We thank the referee who pointed out [4] and A.M. Tyryshkin for his simulation program HYSCORE3.

References

[1] R.R. Ernst, G. Bodenhausen, A. Wokaun, Principles of Nuclear Magnetic Resonance in One and Two Dimensions, Clarendon Press, Oxford, 1987.
[2] A. Schweiger, G. Jeschke, Principles of Pulse Electron Paramagnetic Resonance, University Press, Oxford, 2001.
[3] M. Linder, A. Höhener, R.R. Ernst, Orientation of tensorial interactions determined from two-dimensional NMR powder spectra, J. Chem. Phys. 73 (1980) 4959–4970.
[4] K. Smidt-Rohr, H.W. Spiess, Multidimensional Solid-State NMR and Polymers, Academic Press, London, 1996, Chapter 6.7.3 and Appendix E.
[5] S.A. Dikanov, M.K. Bowman, Cross-peak lineshape of 2-dimensional ESEEM spectra in disordered S=1/2, I = 1/2 spin systems, J. Magn. Reson. A 116 (1995) 125–128;
S.A. Dikanov, A.M. Tyryshkin, M.K. Bowman, Intensity of cross-peaks in HYSCORE spectra of S = 1/2, I = 1/2 spin systems, J. Magn. Reson. 144 (2000) 228–242.
[6] T. Poston, I. Stewart, Catastrophe Theory and Its Applications, Dover Publications, Mineola, NY, 1996;
V.I. Arnold, Catastrophe Theory, Springer, Berlin–NY, 1992.
[7] P. Hofer, A. Grupp, H. Nebenfuhr, M. Mehring, Hyperfine sublevel correlation (hyscore) spectroscopy: a 2D ESR investigation of the squaric acid radical, Chem. Phys. Lett. 132 (1986) 279–282.
[8] B. Epel, D. Goldfarb, Two-dimensional pulsed TRIPLE at 95 GHz, J. Magn. Reson. 146 (2000) 196–203.
[9] D. Goldfarb, B. Epel, H. Zimmermann, G. Jeschke, 2D TRIPLE in orientationally disordered samples—a means to resolve and determine relative orientation of hyperfine tensors, J. Magn. Reson. 168 (2004) 75–87.
[10] D. Goldfarb, V. Kofman, J. Libman, A. Shanzer, R. Rahmatouline, S. Van Doorslaer, A. Schweiger, Double nuclear coherence transfer (DONUT)-HYSCORE: a new tool for the assignment of nuclear frequencies in pulsed EPR experiments, J. Am. Chem. Soc. 120 (1998) 7020–7029.
[11] L. Xiao, M.E. Kellman, Catastrophe map classification of the generalized normal-local transition in Fermi resonance spectra, J. Chem. Phys. 93 (1990) 5805–5820.
[12] C.E. Zaspel, Cusp catastrophe in the ferromagnetic resonance spectrum of a layered ferromagnet, Phys. Rev. B 41 (1990) 786–787.
[13] L.G. Rowan, E.L. Hahn, W.B. Mims, Electron-spin-echo envelope modulation, Phys. Rev. 137 (1965) A61–A71.
[14] S.A. Dikanov, Yu.D. Tsvetkov, Electron Spin Echo Envelope Modulation (ESEEM) Spectroscopy, CRC Press, Boca Raton, 1992.
[15] G.M. Muha, Exact solution of the NQR I = 1 eigenvalue problem for an arbitrary asymmetry parameter and Zeeman field strength and orientation, J. Chem. Phys. 73 (1980) 4139–4140;
G.M. Muha, The Zeeman effect in $S = 1$ systems, J. Magn. Reson. 49 (1982) 431–443.

[16] A.G. Maryasov, M.K. Bowman, Hyperfine sublevel correlation (HYSCORE) spectra for paramagnetic centers with nuclear spin $I = 1$ having isotropic hyperfine interactions, J. Phys. Chem. B 108 (2004) 9412–9420.

[17] W.B. Mims, Envelope modulation in spin-echo experiments, Phys. Rev. B 5 (1972) 2409–2419.

[18] H. Whitney, On singularities of mappings of Euclidian spaces, I. Mappings of the plane into the plane, Ann. Math. 62 (1955) 374–410.

[19] J.G. Broida, S.G. Williamson, Comprehensive Introduction to Linear Algebra, Addison-Wesley, Reading, MA, 1989.

[20] R.G. Larsen, G.J. Gerfen, D.J. Singel, The glories of ESEEM: measuring electron-nuclear dipolar couplings in orientationally disordered solids, Appl. Magn. Reson. 3 (1992) 369–383.

[21] R.T. Song, P.E. Doan, R.J. Gurbiel, B.E. Sturgeon, B.M. Hoffman, Non-Kramers ENDOR and ESEEM of the $S = 2$ ferrous ion of $[Fe(II)EDTA]^{2-}$, J. Magn. Reson. 141 (1999) 291–300.